

A new tri-particle backlighter for high-energy-density plasmas (invited)

Cite as: Rev. Sci. Instrum. **92**, 063524 (2021); <https://doi.org/10.1063/5.0043845>
 Submitted: 11 January 2021 . Accepted: 18 April 2021 . Published Online: 28 June 2021

 Graeme Sutcliffe,  Patrick Adrian,  Jacob Pearcy,  Timothy Johnson,  Neel Kabadi,  Shaherul Haque,  Cody Parker,  Brandon Lahmann,  Johan Frenje,  Maria Gatu-Johnson,  Hong Sio, Fredrick Séguin, Brad Pollock,  John Moody,  Vladmir Glebov, Roger Janezic, Michael Koch,  Richard Petraso, and Chikang Li

COLLECTIONS

Paper published as part of the special topic on [Proceedings of the 23rd Topical Conference on High-Temperature Plasma Diagnostics](#)



View Online



Export Citation



CrossMark

ARTICLES YOU MAY BE INTERESTED IN

[Characterizing x-ray transmission through filters used in high energy density physics diagnostics](#)



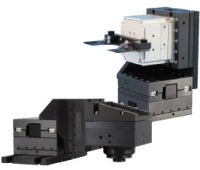
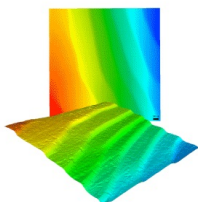
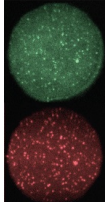
Review of Scientific Instruments **92**, 063502 (2021); <https://doi.org/10.1063/5.0043770>

[High-repetition rate solid target delivery system for PW-class laser-matter interaction at ELI Beamlines](#)

Review of Scientific Instruments **92**, 063504 (2021); <https://doi.org/10.1063/5.0053281>

[Design and implementation of a portable diagnostic system for Thomson scattering and optical emission spectroscopy measurements](#)

Review of Scientific Instruments **92**, 063002 (2021); <https://doi.org/10.1063/5.0043818>

 MCL MAD CITY LABS INC. www.madcitylabs.com	<p>Nanopositioning Systems</p> 	<p>Modular Motion Control</p> 	<p>AFM and NSOM Instruments</p> 	<p>Single Molecule Microscopes</p> 
---	--	--	---	--

A new tri-particle backlighter for high-energy-density plasmas (invited)

Cite as: Rev. Sci. Instrum. 92, 063524 (2021); doi: 10.1063/5.0043845

Submitted: 11 January 2021 • Accepted: 18 April 2021 •

Published Online: 28 June 2021



View Online



Export Citation



CrossMark

Graeme Sutcliffe,^{1,a)} Patrick Adrian,¹ Jacob Percy,¹ Timothy Johnson,¹ Neel Kabadi,¹ Shaherul Haque,¹ Cody Parker,¹ Brandon Lahmann,¹ Johan Frenje,¹ Maria Gatu-Johnson,¹ Hong Sio,¹ Fredrick Séguin,¹ Brad Pollock,² John Moody,² Vladmir Glebov,³ Roger Janezic,³ Michael Koch,³ Richard Petraso,¹ and Chikang Li¹

AFFILIATIONS

¹Massachusetts Institute of Technology, Cambridge, Massachusetts 02139, USA

²Lawrence Livermore National Laboratory, Livermore, California 94550, USA

³Laboratory for Laser Energetics, Rochester, New York 14623, USA

Note: Paper published as part of the Special Topic on Proceedings of the 23rd Topical Conference on High-Temperature Plasma Diagnostics.

^{a)}Author to whom correspondence should be addressed: gdsut@mit.edu

ABSTRACT

A new tri-particle mono-energetic backlighter based on laser-driven implosions of DT^3He gas-filled capsules has been implemented at the OMEGA laser. This platform, an extension of the original D^3He backlighter platform, generates 9.5 MeV deuterons from the T^3He reaction in addition to 14.7 and 3.0 MeV protons from the deuterium and helium-3 reactants. The monoenergetic 14.7 and 3.0 MeV protons have been used with success at OMEGA and the NIF for both radiography and stopping-power studies. There are several advantages of having a third particle to diagnose plasma conditions: an extra time-of-flight-separated radiograph and an improved ability to discern between electric and magnetic fields. In cases where the 3.0 MeV protons cannot penetrate an experiment, the benefit of the additional 9.5 MeV deuterons is magnified. This capability is well-suited for NIF experiments, where large fields and plasma densities often preclude useful 3.0 MeV proton data. The advantages are demonstrated with radiographs of OMEGA plasmas with magnetic and electric fields. Tests using backlighter-scale 420 μm diameter thin glass capsules validate the platform's extended backlighting capability. The performance characteristics of this backlighter, such as source size and timing, are discussed.

Published under an exclusive license by AIP Publishing. <https://doi.org/10.1063/5.0043845>

I. INTRODUCTION

In diagnosing experiments at inertial confinement fusion (ICF) facilities, there is a need to be able to measure magnetic and electric fields inside the small, short-lived high energy density (HED) plasmas. Particularly challenging is the measurement of spatially resolved magnetic and electric fields. Optical techniques such as Faraday rotation have been implemented at ICF facilities but are limited to mean-field measurements in a volume a few hundred micrometers across.¹ Charged particle radiography techniques have been developed over the years to leverage the sensitivity of charged particles to the magnetic and electric fields in the plasmas they traverse.^{2,3} There has been substantial effort in

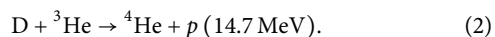
developing sources of energetic charged particles for use in radiography measurements.⁴⁻⁶

ICF facilities have two primary methods to generate charged particles for probing experimental plasmas. One uses a mechanism called *target normal sheath acceleration* (TNSA), whereby a short-pulse laser impinges on the backside of a foil and a proton beam is emitted from the front side with a roughly exponential spectrum.⁴ This technique has a few distinctive features: high spatial and temporal resolution set by the short-pulse laser; a non-uniform, beamed, particle flux; and an exponential continuum of energies up to ~ 60 MeV on OMEGA EP.⁴ In contrast, exploding pusher backlighters have an isotropic proton fluence and have monoenergetic fusion products.⁵ Monoenergetic probe particles can be

an advantage over an exponential spectrum because it avoids degeneracy between deflection from fields and ranging through plasma material and are of particular use when measuring energy downshifts in stopping power experiments.^{7,8}

Fusion backlighters use a shock-dominated implosion platform called an *exploding pusher*.^{9,10} In this class of implosions, lasers heat the shell of a thin-walled glass capsule, ablating the material and launching a shock into the gas fuel. When the shock converges and rebounds, it heats the fuel and fusion occurs in the heated hot spot at the center of the fuel. Charged fusion products can stream out of the fusion volume relatively unperturbed because of the low areal density of the surrounding material.⁸

Fusion reactions in exploding pusher targets provide the quasi-monoenergetic probe particles to probe the experiment. Existing D^3He backlighters employ thin-glass shell capsules roughly $420\ \mu\text{m}$ in diameter. The capsules are filled with 18 atm of equimolar D^3He gas. The fusion of DD and D^3He generates the two quasi-monoenergetic protons for probing experiments: 3 and 14.7 MeV protons through the following reactions:



The fusion product spectra are not perfectly monoenergetic because of Doppler broadening from the thermal motions of the reactants. In a typical backlighter implosion with an ion temperature of 10 keV, the resulting DD-proton and D^3He -proton line spectra have standard deviations of ~ 120 and 240 keV, respectively.

Figure 1 shows a typical experimental configuration on the OMEGA laser. The OMEGA laser has a total of 60 beams, which can provide a combined 30 kJ of 351 nm wavelength light in flexible pulse shapes many nanoseconds long.¹¹ Backlighter capsules are driven with 0.6–1.0 ns duration *square* pulses (nominally constant power with minimum rise and fall times) with a maximum power of 500 GW/beam. The fusion products from the backlighter, which stream through the plasma, are collected on CR-39 detectors. These backlighters have been used with as few as 15 OMEGA beams; however, better performance is achieved with more beams, and recent work has quantified the dependence on laser drive energy and symmetry.¹² Remaining beams are used to drive the experiment.

The new tri-particle backlighter platform extends the capability of the existing D^3He proton backlighter by incorporating tritium as a fuel component. In Sec. II, the tri-particle backlighter and its typical deployment on OMEGA is described. In Sec. III, the results of performance tests are outlined. In Sec. IV, example data and the use of magnetic field reconstruction algorithms are presented. Ongoing and future uses are discussed in Sec. V.

II. THE NEW DT^3He TRI-PARTICLE BACKLIGHTER

By incorporating tritium to the backlighter capsule gas fill, an additional monoenergetic charged particle species is generated through the $T + {}^3He$ nuclear reaction,



A typical charged particle spectrum from the implosion of an $860\ \mu\text{m}$ capsule is shown in Fig. 2(a) with the three quasi-monoenergetic charged fusion products. The particles are detected by CR-39 solid state nuclear track detectors.¹³ A typical detector and filtering stack is shown in Fig. 2(b): $15\ \mu\text{m}$ of tantalum protects the front surface of the CR-39. DD-protons and T^3He -deuterons are recorded on the first $1500\ \mu\text{m}$ CR-39 detector. Additional aluminum filtering ranges down the 14.7 MeV protons to ~ 3 MeV on the second CR-39 piece so that they are in the ~ 1 to 6 MeV energy range that can be detected by CR-39.¹³ The \sim MeV charged particles leave trails of broken molecular bonds in the plastic, which are revealed by chemical etching.¹⁴ The tracks are recorded by an automated microscope scan system.¹³

The DD-protons and the T^3He -deuterons are recorded on the same CR39 piece and thus must be differentiated by track characteristics: diameter and *contrast*, or darkness. Because the DD-protons and T^3He -deuterons have different energy loss rates in the plastic, the resulting track characteristics can be distinguished from each other. The higher energy T^3He -deuterons have fainter, smaller tracks, while the DD-protons have darker, bigger tracks. Figure 2(c) shows a $400\ \mu\text{m}$ microscope frame with roughly $10\ \mu\text{m}$ diameter DD-proton tracks and $2\ \mu\text{m}$ T^3He deuteron tracks.

The change in track characteristics between scan surfaces can be used to further differentiate T^3He deuterons from protons. In the event that the proton and deuteron distributions overlap in diameter space and cannot be differentiated by diameter, a technique that

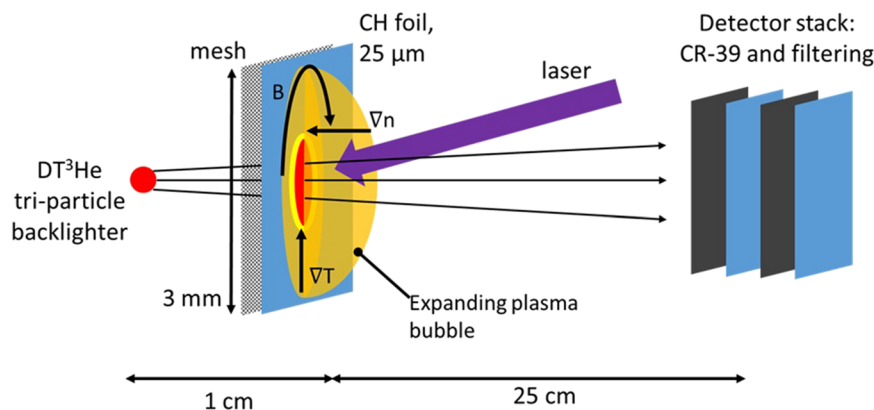


FIG. 1. Typical experimental configuration on OMEGA. About 20 laser beams drive the backlighter capsule. The remaining beams can be used to generate the experimental subject plasma. The probe particles are recorded by CR-39 detectors.

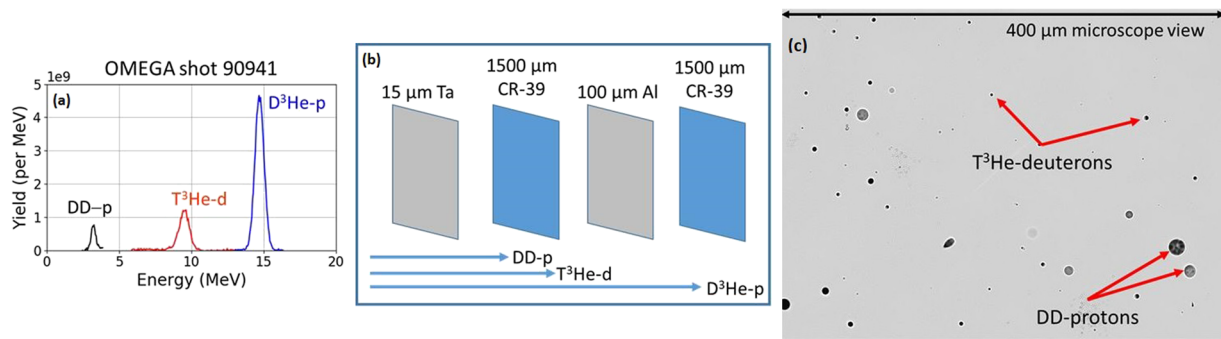


FIG. 2. (a) Spectrum of charged particle fusion products suitable for radiography from a DT³He-filled implosion. The capsule had a D:T:³He fill ratio (atomic) of 5:45:50. (b) Typical detector and filtering stack used. (c) Typical microscope frame shown: The large tracks are DD-protons, while higher-energy T³He-deuterons show up as smaller tracks because they deposit less energy into the CR-39.

looks at the tracks at multiple scan depths can be employed, which is an extension of coincidence-counting background-rejection techniques¹⁵ originally designed to reject neutron backgrounds. First, etching the front surface reveals the DD-proton and T³He-deuteron tracks, which are scanned. Then, the bulk material is removed and the etch/scan process is repeated at the new surface. Tracks on the front surface are paired with their nearest corresponding neighbor on the second surface to generate a histogram of front and back diameters. Because the particle species lose energy at different rates, the protons and deuterons become separated in the two-dimensional diameter space and can be uniquely selected. A study further detailing this method is in progress.¹⁶

DT³He tri-particle backlighter capsules are thin glass (nominally 2 μm thick) and 420 or 860 μm in diameter. Capsules are typically filled with 18 atm of fusion fuel at room temperature, which corresponds to a fill density of roughly 2.5 mg cm⁻³. They are imploded using a subset of the OMEGA laser's 60 beams, using a 0.6 or 1 ns square pulse. The number of charged fusion products (*yield*) can be estimated with the following equation:

$$Y_{ij} = n_i n_j \langle \sigma v \rangle_{ij} \tau V = n^2 f_i f_j \langle \sigma v \rangle_{ij} \tau V, \quad (4)$$

where subscripts *i* and *j* refer to reacting species, *Y* is the total number of particles produced, $n_i = n f_i$ is the number density of species *i*, f_i is the fraction of particles that are species *i*, $\langle \sigma v \rangle_{ij}$ is the fusion reactivity of the reaction of *i* and *j* at a specific temperature, τ is the duration during which reactions occur, and *V* is the volume of fusion reactions. The fusion volume is sensitive primarily to the initial capsule radius and laser drive.^{5,17} The volume and duration of fusion reactions in exploding pusher backlighters do not greatly vary with gas fill density.¹⁷ It has been shown in 860 μm diameter exploding pushers driven with 15 kJ of laser energy on OMEGA that particle yields saturate at fill densities above 1 mg/cm³ because increased fill density results in lower fuel temperatures, and the increase from the factor n^2 is balanced by a decrease in $\langle \sigma v \rangle$ (a function of temperature) in the yield equation.¹⁸ As a result, changing the density (with constant laser power) has little effect on the particle yield. The main parameter that remains is the fraction of the constituent DT³He gas fill. Because the T³He reaction is the lowest in reactivity by about an order of magnitude, the fill must be mostly T³He to compensate and

balance the particle yields. Taking a constant D:T ratio, the T³He and D³He yields are maximized by setting the ³He atomic fraction to 50%. The D content is then chosen such that the DD yields are sufficiently high: Testing in 860 μm diameter capsules on a variety of deuterium fill fractions from 5% to 20% shows that ~10% is the optimal deuterium fraction, and thus, the optimal fill ratio is ~10:40:50 D:T:³He. Because of practical constraints on D:T ratios (the ambient-temperature DT capsule fill station at the OMEGA laser has a fixed D:T ratio), the small-capsule (420 μm) data shown in this work have a fill of 20:30:50 D:T:³He, and the resulting T³He yield is ~75% what it would have been with the optimal fill.

III. DT³He TRI-PARTICLE BACKLIGHTER PERFORMANCE

Qualifying experiments were conducted on OMEGA to assess the key performance characteristics of the tri-particle backlighter. There are four main important parameters. The particle yield dictates the statistically limited smallest resolvable features in a radiograph. Similarly, the size of the fusion volume also puts a lower bound on the smallest resolvable features. The duration of nuclear production dictates the temporal resolution of the system. Finally, the isotropy of particle flux is important in ensuring the overall radiograph quality: Of interest are particle flux variations that result from deflections in the plasma, not those from the spatial structure that arises from the backlighter.

The performance characteristics of the tri-particle backlighter satisfy typical experimental requirements and are outlined in Fig. 3. Figure 3(a) shows the charged particle yields as a function of laser power on capsule. Experiments covered a broad laser power sweep for the large 860 μm targets (the circles) and a more limited sweep for small 420 μm targets (the diamonds). Overall the T³He-deuteron yields are somewhat lower than the D³He-proton yields even after compensation by maximizing T and ³He components of the gas. Figure 3(b) shows the measured production duration of DT neutrons (full-width half-maximum), a proxy measurement of the charged particle production time, and thus the temporal resolution of the system. Measurements for a broad range of laser and capsule parameters show this is between 100 and 200 ps, similar to previous D³He backlighters.⁵ Temporal resolution from the width of the

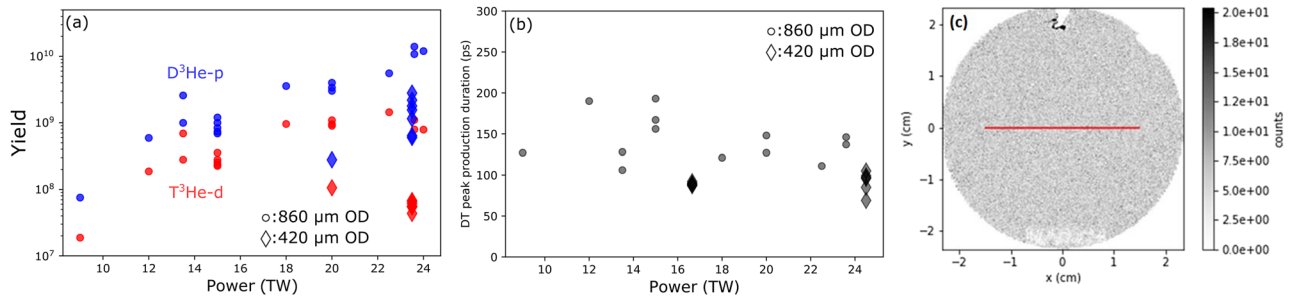


FIG. 3. (a) 4π particle yields measured by wedge range filter (WRF) spectrometers. The circles correspond to large-capsule (nominally $860\ \mu\text{m}$ diameter) implosions, while the diamonds correspond to the smaller capsules (nominally $420\ \mu\text{m}$ diameter). The large capsule D:T: ^3He fill ratios were 5:45:50, while the small capsules had the less optimal 20:30:50 D:T: ^3He because of OMEGA DT fill facility constraints. The yields that are shown have not been adjusted to account for difference in fill fraction between capsules. (b) DT neutron production duration, measured with the neutron temporal diagnostic (NTD).¹⁹ This measurement is a surrogate measurement for the nuclear production duration of charged particles. The measurements show short ($<200\ \text{ps}$) nuclear production duration (full-width half-maximum). (c) Flat-field image of particle distribution on a 4-cm CR-39 detector fielded at 45 cm from the source (subtending $0.025\ \text{sr}$). Variations are statistical, and variations on the scale of the detector size are nearly imperceptible. Variations in particle flux along different lines of sight have been shown to exist in $860\ \mu\text{m}$ exploding pushers and are largely a function of laser timing.²⁰

quasi-monoenergetic spectra is negligible: At worst, the DD-protons have spectral widths $\sim 240\ \text{keV}$ (FWHM) and kinetic energy $3\ \text{MeV}$ and thus have velocities varying on the order of 5%. The time of flight for DD-protons with a typical $1\ \text{cm}$ standoff from the subject is $420\ \text{ps}$, so the breadth of the DD-proton spectrum contributes to $20\ \text{ps}$ of probe time differences. A demonstration of the isotropy of the backlighter is shown in Fig. 3(c). The variations in this small $4\ \text{cm}$ flat-field measurement of the particle flux are almost entirely statistical, and the particle density on a large scale is uniform. Finally, in experiments with $20\ \text{TW}$ power on capsules, the fusion source radii were measured using the Proton Core Imaging System (PCIS).²¹ The T^3He -deuteron and D^3He -proton source radii were measured to be $80 \pm 10\ \mu\text{m}$ and $70 \pm 10\ \mu\text{m}$, respectively, lining up with previously measured trends of D^3He -proton source volumes.¹⁷ Importantly, the backlighter parameters can be tailored to experimental need: If yield is more important than imaging resolution, $860\ \mu\text{m}$ capsules can be used instead of $420\ \mu\text{m}$ capsules to improve particle yields.

IV. RADIOGRAPHY DEMONSTRATION EXPERIMENTS

To demonstrate the radiography capabilities of the tri-particle backlighter, the data were collected using an experimental setup shown in Fig. 1. Capsules with a diameter of $860\ \mu\text{m}$ were filled at

room temperature with $12\ \text{atm}$ of DT^3He gas with an atomic ratio of 20:40:40 D:T: ^3He . The capsules were driven by 59 OMEGA beams with a pulse duration of $0.6\ \text{ns}$ and a total on-capsule energy of $\sim 25\ \text{kJ}$. A mesh collimates the particles into beamlets. A $25\ \mu\text{m}$ thick CH foil is impinged on by a laser, generating a plasma bubble. Because of the non-parallel density and temperature gradients, a magnetic field is generated, which is oriented azimuthally around the bubble. The particles that pass through the bubble are collected onto the detector stack.

The data recorded by the detector stack are shown in Fig. 4. Because the particle species have different velocities, each species has a different time-of-flight delay, which causes the probe times to be different. The $14.7\ \text{MeV}$ D^3He -protons arrive at the plasma first, followed by the $9.5\ \text{MeV}$ T^3He -deuterons and then the $3\ \text{MeV}$ DD-protons. The DD-proton has lost the spatial information of the beamlets because of the scattering in the CH foil and plasma.

The three particles have different masses and energies, leading to different sensitivities to fields and scattering,

$$\theta_B \propto qBL/\sqrt{mE}, \tag{5}$$

$$\theta_E \propto qEL/E, \tag{6}$$

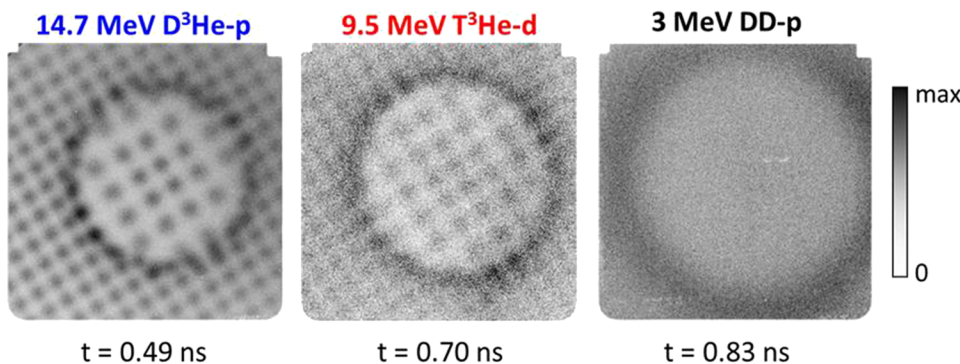


FIG. 4. Data from mesh-generated beamlets of different particle groups. The radiographs are arranged left-to-right in the order of time-of-flight arrival at plasma subject: D^3He -protons, then T^3He -deuterons, and then DD-protons.

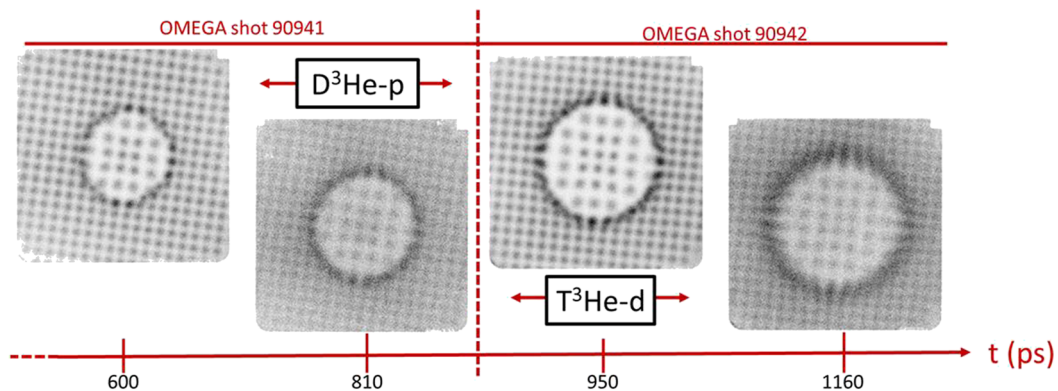


FIG. 5. Data from mesh-generated beamlets of different particle groups for two different OMEGA shots of the nominally same subject plasma. D³He-proton and T³He-deuteron radiographs are arranged left-to-right in the order of time-of-flight arrival at plasma subject with $t = 0$ ps corresponding to the time that the subject plasma drive beam turned on. The integration time of each image is dominated by a source burn duration of 150 ps.

$$\theta_{\text{scattering}} \propto q^2 nL/E, \quad (7)$$

where θ is the deflection angle of a particle under a field/scattering, B is the magnetic field, \mathcal{E} is the electric field, n is the plasma electron density, L is the path length through plasma, q is the particle charge, m is the particle mass, and E is the particle energy. The comparison of the deflections experienced by different particle species can be used to infer whether the particles were deflected by magnetic or electric fields or by scattering in the plasma. For example, we expect the 3 MeV DD-proton, the lowest energy particle, to be most influenced by scattering in the plasma, and this can be seen in the data: The DD-proton flux has been smoothed by scattering in the foil and plasma. The D³He-proton and T³He-deuteron retain more of their spatial information because of their higher energy. The 9.5 MeV T³He-deuteron is especially useful in environments where fields and plasma scattering are too strong for the DD-proton to produce a quality radiograph (for example, hohlraum experiments).

The radiographs capture the evolution of fields on timescales of order 100 ps by leveraging the time-of-flight separation of the

particles. Figure 5 shows data from two separate shots where spatial resolution has not been reduced by scattering: The data would have been limited to single probe time per shot with the 14.7 MeV proton if the D³He backlighter had been used. With the tri-particle backlighter, the amount of time-resolved data is doubled and importantly single-shot time-evolution measurements are captured. This can be important in experiments where there is large shot-to-shot variation in the plasma structures and it is necessary to identify the single-shot evolution of plasma structures, such as in recent OMEGA experiments replicating the dynamics of the Crab Nebula pulsar magnetized jet experiments²² [see the measurement of jet velocity in Figs. 1 and 5(a)]. In cases where all three particles provide useful information, the third time-of-flight separated particle could provide second-time-derivative measurements of quantities such as velocity or magnetic field growth.

New field reconstruction techniques,^{23–26} which back out spatially resolved fields from radiographs, stand to benefit from the new probe particle. The reconstruction shown in Fig. 6 uses an *optimal transport* algorithm to deduce particle deflections^{23,25,26} and converts these spatially resolved deflections under the assumption that they

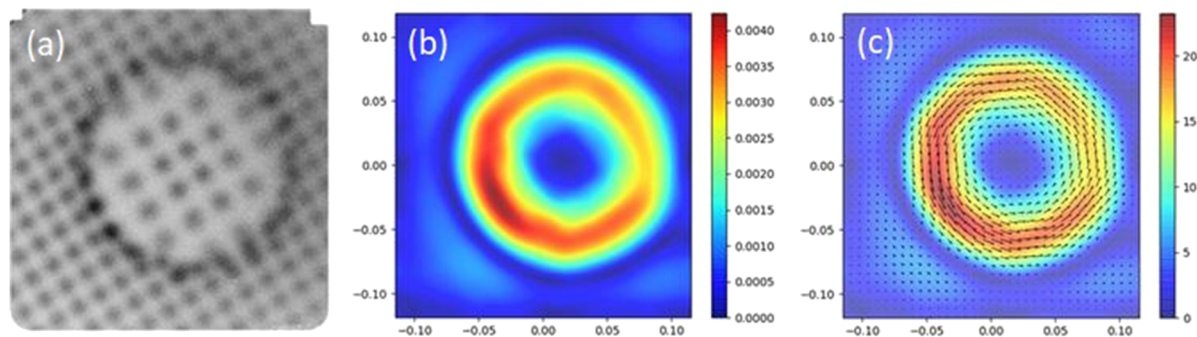


FIG. 6. (a) D³He-proton radiograph, which was then low-pass filtered in preprocessing to remove beamlet structure but maintain the overall structure from magnetic field deflections. (b) Algorithm-inferred deflection field magnitude. The deflection map is a vector-valued field describing the amplitude and direction of particle deflections as a function of space. (c) Path-integrated transverse magnetic field sampled by the probe particles, $B_{\perp}L$ (in megagauss-micrometers). The arrows represent the direction and magnitude of the reconstructed field.

are caused by magnetic fields. Preprocessing the input data must be done carefully as it can have an impact on the final results; cross-checking reconstruction results between different particle species is a way to ensure that preprocessing inputs are not having a large effect on resulting radiographs and is a key reason why having multiple independent radiographs is useful. Future extensions to the algorithm will seek to address unfolding of deflections under electric fields, magnetic fields, and plasma scattering, which is only possible by having the three independent particle radiographs to provide the different sensitivities required to back out the relative strengths of the deflection mechanisms.

V. CURRENT AND FUTURE USES OF THE TRI-PARTICLE BACKLIGHTER

Outlined here are examples of ongoing and future uses of the tri-particle backlighter. The tri-particle backlighter is being used to untangle magnetic and electric fields in an high-field, high-scattering environment: hohlraums. Previous experiments²⁷ explored the dominant fields in vacuum and gas filled hohlraums as seen by 14.7 MeV proton radiographs. The conclusion, consistent with the structure in the radiographs, was that electric fields associated with electron pressure gradients were the main cause of the deflections of the protons. These measurements could not, however, rely on deflection scaling arguments by comparing to DD-proton radiographs because the hohlraum environment was too dense and the fields were too strong for the protons to make it through the experiment to the detector.²⁷ Ongoing work utilizes the new $T^3\text{He}$ -deuteron from the tri-particle backlighter in vacuum and gas filled hohlraums to leverage the two-particle deflection scaling approach to address this problem. Stopping power measurements of warm dense matter⁷ and other laser-generated plasmas⁸ would benefit from using both the $D^3\text{He}$ -proton and $T^3\text{He}$ -deuteron as probe particles: By making simultaneous stopping measurements, some of the systematic shot-to-shot variations such as variations in target manufacturing and laser to x-ray conversion could be accounted for, potentially reducing the overall measurement uncertainty. Such a measurement is not feasible using the DD-proton alongside the $D^3\text{He}$ -proton because experimental subjects with sufficient trajectory-integrated density to resolve a measurable energy downshift in the $D^3\text{He}$ -proton result in blocking the DD-proton completely. Another use case is the measurement of fields in laser-driven coils²⁸ and MIFEDs coils,²⁹ both of which are currently being used in magnetized ICF research.³⁰

VI. CONCLUSION

To summarize, a new tri-particle backlighter platform that extends the capability of the existing $D^3\text{He}$ proton backlighter has been developed and tested. The test results show that the performance of the tri-particle backlighter matches key aspects of the $D^3\text{He}$ platform. The additional $T^3\text{He}$ -deuteron provides a third time-of-flight separated probe of experiments. The deuteron's unique deflection under magnetic and electric fields provides a further means to distinguish between them, and its lower deflection under plasma scattering than the DD-proton means that denser plasmas may be probed before spatial resolution is lost. The new data could, in principle, be leveraged in the next generation of field reconstruction algorithms to unfold the spatially resolved magnetic

fields, electric fields, and plasma scattering environment probed by the particles.

ACKNOWLEDGMENTS

The authors thank research specialists Bob Frankel and Ernie Doeg who were responsible for the processing of the CR-39 data. This work was supported, in part, by the U.S. Department of Energy NNSA MIT Center-of-Excellence under Contract No. DE-NA0003868 and by NLUF. This report was prepared as an account of work sponsored by an agency of the United States Government. Neither the United States Government nor any agency thereof, nor any of their employees, makes any warranty, express or implied, or assumes any legal liability or responsibility for the accuracy, completeness, or usefulness of any information, apparatus, product, or process disclosed, or represents that its use would not infringe privately owned rights. Reference herein to any specific commercial product, process, or service by trade name, trademark, manufacturer, or otherwise does not necessarily constitute or imply its endorsement, recommendation, or favoring by the United States Government or any agency thereof. The views and opinions of authors expressed herein do not necessarily state or reflect those of the United States Government or any agency thereof.

DATA AVAILABILITY

The data that support the findings of this study are available from the corresponding author upon reasonable request.

REFERENCES

- 1 A. Rigby, J. Katz, A. F. A. Bott, T. G. White, P. Tzeferacos, D. Q. Lamb, D. H. Froula, and G. Gregori, *High Power Laser Sci. Eng.* **6**, e49 (2018).
- 2 A. J. Mackinnon, P. K. Patel, R. P. Town, M. J. Edwards, T. Phillips, S. C. Lerner, D. W. Price, D. Hicks, M. H. Key, S. Hatchett, S. C. Wilks, M. Borghesi, L. Romagnani, S. Kar, T. Toncian, G. Pretzler, O. Willi, M. Koenig, E. Martinolli, S. Lepape, A. Benuzzi-Mounaix, P. Audebert, J. C. Gauthier, J. King, R. Snavely, R. R. Freeman, and T. Boehlly, *Rev. Sci. Instrum.* **75**, 3531–3536 (2004).
- 3 L. Romagnani, J. Fuchs, M. Borghesi, P. Antici, P. Audebert, F. Ceccherini, T. Cowan, T. Grismayer, S. Kar, A. MacChi, P. Mora, G. Pretzler, A. Schiavi, T. Toncian, and O. Willi, *Phys. Rev. Lett.* **95**, 195001 (2005).
- 4 K. Flippo, T. Bartal, F. Beg, S. Chawla, J. Cobble, S. Gaillard, D. Hey, A. MacKinnon, A. MacPhee, P. Nilson, D. Offermann, S. L. Pape, and M. J. Schmitt, *J. Phys.: Conf. Ser.* **244**, 022033 (2010).
- 5 C. K. Li, F. H. Séguin, J. A. Frenje, J. R. Rygg, R. D. Petrasso, R. P. Town, P. A. Amendt, S. P. Hatchett, O. L. Landen, A. J. MacKinnon, P. K. Patel, V. A. Smalyuk, J. P. Knauer, T. C. Sangster, and C. Stoeckl, *Rev. Sci. Instrum.* **77**, 10E725 (2006).
- 6 J. R. Rygg, A. B. Zylstra, F. H. Séguin, S. Lepape, B. Bachmann, R. S. Craxton, E. M. Garcia, Y. Z. Kong, M. Gatu-Johnson, S. F. Khan, B. J. Lahmann, P. W. McKenty, R. D. Petrasso, H. G. Rinderknecht, M. J. Rosenberg, D. B. Sayre, and H. W. Sio, *Rev. Sci. Instrum.* **86**, 116104 (2015).
- 7 A. B. Zylstra, J. A. Frenje, P. E. Grabowski, C. K. Li, G. W. Collins, P. Fitzsimmons, S. Glenzer, F. Graziani, S. B. Hansen, S. X. Hu, M. G. Johnson, P. Keiter, H. Reynolds, J. R. Rygg, F. H. Séguin, and R. D. Petrasso, *Phys. Rev. Lett.* **114**, 215002 (2015).
- 8 J. A. Frenje, R. Florido, R. Mancini, T. Nagayama, P. E. Grabowski, H. Rinderknecht, H. Sio, A. Zylstra, M. G. Johnson, C. K. Li, F. H. Séguin, R. D. Petrasso, V. Y. Glebov, and S. P. Regan, *Phys. Rev. Lett.* **122**, 015002 (2019).
- 9 E. K. Storm, H. G. Ahlstrom, M. J. Boyle, D. E. Campbell, L. W. Coleman, S. S. Glaros, H. N. Kornblum, B. Lerche, D. B. MacQuigg, D. W. Phillion, F. Bainer, B. Bienecker, V. C. Rupert, V. W. Slivinsky, D. B. Speck, C. D. Swift, and K. G. Tirsell, *Phys. Rev. Lett.* **40**, 1570 (1978).

- ¹⁰M. D. Rosen and J. H. Nuckolls, *Phys. Fluids* **22**, 1393 (1979).
- ¹¹T. R. Boehly, R. S. Craxton, T. H. Hinterman, J. H. Kelly, T. J. Kessler, S. A. Kumpan, S. A. Letzring, R. L. McCrory, S. F. B. Morse, W. Seka, S. Skupsky, J. M. Soures, and C. P. Verdon, *Rev. Sci. Instrum.* **66**, 508 (1995).
- ¹²T. M. Johnson, A. Birkel, H. Ramirez, G. D. Sutcliffe, P. J. Adrian, V. Y. Glebov, H. Sio, M. G. Johnson, J. Frenje, R. Petrasso, and C. Li, *Rev. Sci. Instrum.* **92**, 043551 (2021).
- ¹³F. H. Séguin, J. A. Frenje, C. K. Li, D. G. Hicks, S. Kurebayashi, J. R. Rygg, B.-E. Schwartz, R. D. Petrasso, S. Roberts, J. M. Soures, D. D. Meyerhofer, T. C. Sangster, J. P. Knauer, C. Sorce, V. Y. Glebov, C. Stoeckl, T. W. Phillips, R. J. Leeper, K. Fletcher, and S. Padalino, *Rev. Sci. Instrum.* **74**, 975 (2003).
- ¹⁴J. Charvát and F. Spurný, *Nucl. Tracks Radiat. Meas.* **14**, 447–449 (1988).
- ¹⁵D. T. Casey, J. A. Frenje, F. H. Séguin, C. K. Li, M. J. Rosenberg, H. Rinderknecht, M. J. Manuel, M. G. Johnson, J. C. Schaeffer, R. Frankel, N. Sinenian, R. A. Childs, R. D. Petrasso, V. Y. Glebov, T. C. Sangster, M. Burke, and S. Roberts, *Rev. Sci. Instrum.* **82**, 073502 (2011).
- ¹⁶S. Haque, G. Sutcliffe, B. Lahmann, M. G. Johnson, R. Petrasso, and C. Li, “A technique to discriminate between particle species in CR-39 detectors,” *Rev. Sci. Instrum.* (unpublished) (2021).
- ¹⁷F. H. Séguin, J. L. Deciantis, J. A. Frenje, C. K. Li, J. R. Rygg, C. D. Chen, R. D. Petrasso, J. A. Delettrez, S. P. Regan, V. A. Smalyuk, V. Y. Glebov, J. P. Knauer, F. J. Marshall, D. D. Meyerhofer, S. Roberts, T. C. Sangster, C. Stoeckl, K. Mikaelian, H. S. Park, H. F. Robey, and R. E. Tipton, *Phys. Plasmas* **13**, 082704 (2006).
- ¹⁸M. J. Rosenberg, H. G. Rinderknecht, N. M. Hoffman, P. A. Amendt, S. Atzeni, A. B. Zylstra, C. K. Li, F. H. Séguin, H. Sio, M. G. Johnson, J. A. Frenje, R. D. Petrasso, V. Y. Glebov, C. Stoeckl, W. Seka, F. J. Marshall, J. A. Delettrez, T. C. Sangster, R. Betti, V. N. Goncharov, D. D. Meyerhofer, S. Skupsky, C. Bellei, J. Pino, S. C. Wilks, G. Kagan, K. Molvig, and A. Nikroo, *Phys. Rev. Lett.* **112**, 185001 (2014).
- ¹⁹C. Stoeckl, R. Boni, F. Ehrne, C. J. Forrest, V. Y. Glebov, J. Katz, D. J. Lonobile, J. Magoon, S. P. Regan, M. J. Shoup, A. Sorce, C. Sorce, T. C. Sangster, and D. Weiner, *Rev. Sci. Instrum.* **87**, 053501 (2016).
- ²⁰C. J. Waugh, M. J. Rosenberg, A. B. Zylstra, J. A. Frenje, F. H. Séguin, R. D. Petrasso, V. Y. Glebov, T. C. Sangster, and C. Stoeckl, *Rev. Sci. Instrum.* **86**, 053506 (2015).
- ²¹J. L. DeCiantis, F. H. Séguin, J. A. Frenje, V. Berube, M. J. Canavan, C. D. Chen, S. Kurebayashi, C. K. Li, J. R. Rygg, B. E. Schwartz, R. D. Petrasso, J. A. Delettrez, S. P. Regan, V. A. Smalyuk, J. P. Knauer, F. J. Marshall, D. D. Meyerhofer, S. Roberts, T. C. Sangster, C. Stoeckl, K. Mikaelian, H. S. Park, and H. F. Robey, *Rev. Sci. Instrum.* **77**, 043503 (2006).
- ²²C. K. Li, P. Tzeferacos, D. Lamb, G. Gregori, P. A. Norreys, M. J. Rosenberg, R. K. Follett, D. H. Froula, M. Koenig, F. H. Seguin, J. A. Frenje, H. G. Rinderknecht, H. Sio, A. B. Zylstra, R. D. Petrasso, P. A. Amendt, H. S. Park, B. A. Remington, D. D. Ryutov, S. C. Wilks, R. Betti, A. Frank, S. X. Hu, T. C. Sangster, P. Hartigan, R. P. Drake, C. C. Kuranz, S. V. Lebedev, and N. C. Woolsey, *Nat. Commun.* **7**, 13081 (2016).
- ²³M. M. Sulman, J. F. Williams, and R. D. Russell, *Appl. Numer. Math.* **61**, 298 (2011).
- ²⁴N. L. Kugland, D. D. Ryutov, C. Plechaty, J. S. Ross, and H. S. Park, *Plasma Phys. Controlled Fusion* **54**, 105021 (2012).
- ²⁵M. F. Kasim, L. Ceurvorst, N. Ratan, J. Sadler, N. Chen, A. Sävert, R. Trines, R. Bingham, P. N. Burrows, M. C. Kaluza, and P. Norreys, *Phys. Rev. E* **95**, 023306 (2017).
- ²⁶A. F. Bott, C. Graziani, P. Tzeferacos, T. G. White, D. Q. Lamb, G. Gregori, and A. A. Schekochihin, *J. Plasma Phys.* **83**, 905830614 (2017).
- ²⁷C. K. Li, F. H. Séguin, J. A. Frenje, R. D. Petrasso, P. A. Amendt, R. P. Town, O. L. Landen, J. R. Rygg, R. Betti, J. P. Knauer, D. D. Meyerhofer, J. M. Soures, C. A. Back, J. D. Kilkenny, and A. Nikroo, *Phys. Rev. Lett.* **102**, 205001 (2009).
- ²⁸L. Gao, H. Ji, G. Fiksel, W. Fox, M. Evans, and N. Alfonso, *Phys. Plasmas* **23**, 043106 (2016).
- ²⁹G. Fiksel, A. Agliata, D. Barnak, G. Brent, P. Y. Chang, L. Folsnbee, G. Gates, D. Hasset, D. Lonobile, J. Magoon, D. Mastro Simone, M. J. Shoup, and R. Betti, *Rev. Sci. Instrum.* **86**, 016105 (2015).
- ³⁰M. Hohenberger, P. Y. Chang, G. Fiksel, J. P. Knauer, R. Betti, F. J. Marshall, D. D. Meyerhofer, F. H. Séguin, and R. D. Petrasso, *Phys. Plasmas* **19**, 056306 (2012).